Zeitschrift: Helvetica Physica Acta
Band: 64 (1991)
Heft: 5

Artikel: A new analysis of PSI pp d^+ data
Autor: Cantale, G. / Gaillard, G. / Heer, E.
DOI: https://doi.org/10.5169/seals-116320

Nutzungsbedingungen
Die ETH-Bibliothek ist die Anbieterin der digitalisierten Zeitschriften auf E-Periodica. Sie besitzt keine Urheberrechte an den Zeitschriften und ist nicht verantwortlich für deren Inhalte. Die Rechte liegen in der Regel bei den Herausgebern beziehungsweise den externen Rechteinhabern. Das Veröffentlichen von Bildern in Print- und Online-Publikationen sowie auf Social Media-Kanälen oder Webseiten ist nur mit vorheriger Genehmigung der Rechteinhaber erlaubt. Mehr erfahren

Conditions d'utilisation
L'ETH Library est le fournisseur des revues numérisées. Elle ne détient aucun droit d'auteur sur les revues et n'est pas responsable de leur contenu. En règle générale, les droits sont détenus par les éditeurs ou les détenteurs de droits externes. La reproduction d'images dans des publications imprimées ou en ligne ainsi que sur des canaux de médias sociaux ou des sites web n'est autorisée qu'avec l'accord préalable des détenteurs des droits. En savoir plus

Terms of use
The ETH Library is the provider of the digitised journals. It does not own any copyrights to the journals and is not responsible for their content. The rights usually lie with the publishers or the external rights holders. Publishing images in print and online publications, as well as on social media channels or websites, is only permitted with the prior consent of the rights holders. Find out more

Download PDF: 01.12.2025

ETH-Bibliothek Zürich, E-Periodica, https://www.e-periodica.ch

Helvetica Physica Acta
Vol. 64 (1991)

0018-0238/91/050736-23$1.50+0.20/0
(c) 1991 Birkhäuser Verlag, Basel

A New Analysis of PSI $\vec{p}p \rightarrow \vec{d}\pi^+$ Data

G. Cantale, G. Gaillard, E. Heer, R. Hess, C. Lechanoine-Leluc and D. Rapin

DPNC, Université de Genève, CH-1211 GENEVE 4, Switzerland

(5. III. 1991, revised 13. V. 1991)

Abstract

In 1987, the Geneva group published the first direct reconstruction of the six complex amplitudes of the $pp \rightarrow d\pi^+$ reaction at 447, 515 and 580 MeV. This reconstruction was based on spin correlation and spin transfer observables measured at PSI. Since, due to a sign disagreement with the K_{SS} data recently measured at TRIUMF, we discovered that some of our spin transfer parameters had a sign error. This paper details the new analysis performed with the corrected data. We took advantage of this new analysis to improve the d–C polarimeter analysing powers treatment and to make a comparison with new available theoretical models.

1 Introduction

In 1987, the Geneva group published an article [1] in which the deuteron vectorial and tensorial polarizations, induced by spin transfer mechanisms in the $\vec{p}p \rightarrow \vec{d}\pi^+$ reaction, were presented. Theses results, added to previous spin correlation and analysing powers measurements [2,3], allowed to directly reconstruct the $pp \rightarrow d\pi^+$ amplitudes at 8 deuteron center-of-mass angles between 50° and 90° at 447, 515 and 580 MeV. This was the first time that a model-independent reconstruction of the 6 complex amplitudes of the $pp \rightarrow d\pi^+$ reaction was achieved. A partial wave analysis (PWA) was also performed over the full angular range.

In 1988, first preliminary results of the spin-transfer parameter K_{SS} measurement, performed at TRIUMF at 510 MeV, appeared. Theses results, now published [4], were in disagreement with the PSI measurements. Independently, Prof. D. Bugg called our attention to the difficulties he had in introducing some of our spin transfer data in his PWA and on the possibility of a sign error in some of the data [5].

The origin of the discrepancies is now well understood. In the following section, we will discuss the consequences on the PSI data. A brief description of the analysis will be given in section 3. The consequences on the amplitudes will be explained in section 4. In section 5, the new amplitude analysis will be presented and the results compared to theoretical calculations in section 6.

2 Data Correction

After many cross-checks, it turned out that the problem was due to an error in the sign of the longitudinal and sideways polarizations of the primary proton beam, which occured during the analysis of the spin transfer data. This error was uncovered by studying the p–p elastic data that were taken at the same time that the $pp \rightarrow d\pi^+$ data in order to check out for some eventual instrumental asymmetries. One clearly had to reverse the signs of the longitudinal and sideways beam polarizations to obtain the correct signs for the $\sin(\phi)$ terms in the polarimeter scattering distribution for $\vec{p}p \rightarrow \vec{p}p$ elastic scattering. The effect of this change of sign on the $pp \rightarrow d\pi^+$ data is to reverse the signs of $\varepsilon_s(X)$, $\varepsilon_{2s}(X)$, $\varepsilon_s(Z)$ and $\varepsilon_{2s}(Z)$. The correct values are given in tables 1 to 4 which replace tables 7 to 10 of ref. [1]. In fact, for the diligent reader, it is necessary to state that in tables 7 and 8 of ref. [1] there was moreover a transcription error at 580 MeV affecting the sign of these asymmetries. Nevertheless figures

$\theta_{\text{c.m.}}$[deg.]	447 MeV	515 MeV	580 MeV
52.50	0.0325 ± 0.0083	-0.0095 ± 0.0075	-0.0425 ± 0.0044
57.50	0.0327 ± 0.0066	0.0043 ± 0.0068	-0.0465 ± 0.0039
62.50	0.0228 ± 0.0058	-0.0013 ± 0.0061	-0.0310 ± 0.0041
67.50	0.0252 ± 0.0068	0.0018 ± 0.0069	-0.0282 ± 0.0044
72.50	0.0175 ± 0.0068	0.0105 ± 0.0069	-0.0228 ± 0.0047
77.50	0.0102 ± 0.0078	-0.0186 ± 0.0070	-0.0073 ± 0.0049
82.50	0.0064 ± 0.0098	0.0003 ± 0.0094	-0.0039 ± 0.0051
87.50	0.0075 ± 0.0143	-0.0042 ± 0.0041	-0.0109 ± 0.0063
92.50			-0.0232 ± 0.0097
93.75	-0.0096 ± 0.0094	-0.0212 ± 0.0101	
97.50			-0.0327 ± 0.0076
101.25	-0.0222 ± 0.0070	-0.0266 ± 0.0073	
102.50			-0.0296 ± 0.0072
107.50			-0.0497 ± 0.0066
108.75	-0.0221 ± 0.0066	-0.0296 ± 0.0060	
112.50			-0.0546 ± 0.0060
116.25	-0.0187 ± 0.0056	-0.0301 ± 0.0059	
117.50			-0.0436 ± 0.0055
122.50			-0.0474 ± 0.0050
123.75	-0.0087 ± 0.0050	-0.0278 ± 0.0055	
127.50			-0.0365 ± 0.0047
131.25	-0.0160 ± 0.0048	-0.0278 ± 0.0044	
132.50			-0.0236 ± 0.0044
137.50			-0.0262 ± 0.0042
138.75	-0.0074 ± 0.0067	-0.0088 ± 0.0054	
142.50			-0.0242 ± 0.0041
146.25	0.0252 ± 0.0359	-0.0065 ± 0.0147	
147.50			-0.0165 ± 0.0049

Table 1: Numerical values for the measured asymmetry $\varepsilon_s(X)$ at 447, 515 and 580 MeV as a function of the deuteron center of mass angle.

9 and 10 plotting the measured asymmetries at the 3 energies are all consistent, therefore a reversal of sign has to be applied to all of them. To ensure a clear understanding, we give in this article the corrected tables, and only these should be considered. It leaves untouched $\varepsilon_c(0)$, $\varepsilon_{2c}(0)$, $\varepsilon_c(+y)$, $\varepsilon_{2c}(+y)$, $\varepsilon_c(-y)$, $\varepsilon_{2c}(-y)$ (given in tables 4 to 6 of ref. [1]) and, of course, the spin correlation coefficients and analysing powers previously measured.

3 Description of the Amplitude Analysis

A detailed description of the amplitude analysis can be found in ref. [1] but, for clarity, we will recall here its main features.

Six independent complex amplitudes are necessary to describe the $pp \rightarrow d\pi^+$ scattering matrix. In principle, their knowledge requires the measurement of 11 independent observables, one overall phase remaining arbitrary. In practice, a larger number of observables is

$\theta_{c.m.}$[deg.]	447 MeV	515 MeV	580 MeV
52.50	-0.0189 ± 0.0081	-0.0193 ± 0.0079	-0.0031 ± 0.0043
57.50	-0.0141 ± 0.0065	-0.0234 ± 0.0056	-0.0163 ± 0.0039
62.50	-0.0232 ± 0.0062	-0.0260 ± 0.0063	-0.0123 ± 0.0041
67.50	-0.0225 ± 0.0054	-0.0192 ± 0.0058	-0.0176 ± 0.0044
72.50	-0.0282 ± 0.0067	-0.0137 ± 0.0063	-0.0121 ± 0.0046
77.50	-0.0243 ± 0.0077	-0.0245 ± 0.0077	-0.0185 ± 0.0048
82.50	-0.0262 ± 0.0096	-0.0187 ± 0.0092	-0.0159 ± 0.0050
87.50	0.0073 ± 0.0141	-0.0288 ± 0.0140	0.0055 ± 0.0062
92.50			-0.0087 ± 0.0097
93.75	-0.0171 ± 0.0093	-0.0067 ± 0.0108	
97.50			-0.0150 ± 0.0076
101.25	-0.0296 ± 0.0067	-0.0125 ± 0.0081	
102.50			-0.0032 ± 0.0071
107.50			-0.0077 ± 0.0065
108.75	-0.0168 ± 0.0053	-0.0106 ± 0.0072	
112.50			-0.0008 ± 0.0059
116.25	-0.0118 ± 0.0048	-0.0030 ± 0.0056	
117.50			-0.0129 ± 0.0054
122.50			-0.0040 ± 0.0050
123.75	-0.0102 ± 0.0050	-0.0203 ± 0.0046	
127.50			-0.0102 ± 0.0046
131.25	-0.0119 ± 0.0043	-0.0057 ± 0.0048	
132.50			-0.0090 ± 0.0043
137.50			-0.0081 ± 0.0041
138.75	-0.0096 ± 0.0060	-0.0054 ± 0.0052	
142.50			-0.0101 ± 0.0040
146.25	-0.0188 ± 0.0297	-0.0168 ± 0.0148	
147.50			-0.0058 ± 0.0047

Table 2: Same as Table 1 but for $\varepsilon_{2s}(X)$.

needed in order to avoid multiple solutions due to experimental uncertainties. At one given angle, there exist only 7 independent quantities involving polarization only in the initial state (or no polarization) : the differential cross section $d\sigma/d\Omega$, the analysing powers A_{yo} and A_{oy} and the spin correlation parameters A_{xx}, A_{yy}, A_{zz} and A_{zx}. Therefore, the measurement of parameters dependent on the outgoing deuteron polarization is required to obtain a complete set of observables, allowing a direct and model–independent reconstruction of the scattering matrix.

By means of different combinations of solenoids and dipoles, normal, longitudinal and sideways polarizations could be achieved for the PSI proton beam. By rescattering the outgoing deuterons from a carbon slab, 10 independent asymmetries ε's, depending on the first and second scattering, could be measured. Together with the differential cross section, 2 analysing powers and 4 spin correlation coefficients previously measured at PSI by the Geneva group [6,2,3], this raised the number of available independent observables to 17. But the asymmetries depend on the polarimeter analysing powers iT_{11}, T_{20}, T_{21} and T_{22} which

$\theta_{c.m.}$[deg.]	447 MeV	515 MeV	580 MeV
52.50	0.0930 ± 0.0086	0.1064 ± 0.0074	0.1173 ± 0.0044
57.50	0.0788 ± 0.0070	0.0940 ± 0.0068	0.0995 ± 0.0041
62.50	0.0627 ± 0.0063	0.0776 ± 0.0060	0.0779 ± 0.0044
67.50	0.0649 ± 0.0072	0.0569 ± 0.0069	0.0633 ± 0.0048
72.50	0.0517 ± 0.0072	0.0484 ± 0.0069	0.0356 ± 0.0052
77.50	0.0339 ± 0.0083	0.0132 ± 0.0070	0.0242 ± 0.0055
82.50	0.0227 ± 0.0105	0.0103 ± 0.0094	0.0102 ± 0.0059
87.50	0.0091 ± 0.0155	-0.0060 ± 0.0139	0.0020 ± 0.0072
92.50			-0.0039 ± 0.0092
93.75	0.0091 ± 0.0093	-0.0098 ± 0.0107	
97.50			0.0116 ± 0.0074
101.25	0.0046 ± 0.0070	-0.0081 ± 0.0076	
102.50			0.0164 ± 0.0070
107.50			0.0193 ± 0.0065
108.75	0.0008 ± 0.0066	0.0048 ± 0.0063	
112.50			0.0178 ± 0.0059
116.25	-0.0006 ± 0.0056	0.0123 ± 0.0061	
117.50			0.0275 ± 0.0055
122.50			0.0291 ± 0.0050
123.75	0.0106 ± 0.0051	-0.0018 ± 0.0056	
127.50			0.0220 ± 0.0046
131.25	-0.0005 ± 0.0049	0.0106 ± 0.0046	
132.50			0.0275 ± 0.0044
137.50			0.0194 ± 0.0041
138.75	-0.0061 ± 0.0070	-0.0025 ± 0.0057	
142.50			0.0079 ± 0.0041
146.25	-0.0153 ± 0.0398	0.0009 ± 0.0151	
147.50			0.0098 ± 0.0050

Table 3: Same as Table 1 but for $\varepsilon_s(Z)$.

were unknown and had to be taken as free parameters in the analysis, in the same way as the amplitudes (we are following here the Madison convention for the definition of the analysing powers, which was not the case in ref. [1]). In fact, we will explain in section 5 that one has reasons to take T_{20} equal to 0. Thus, 14 parameters would have to be fitted by means of 17 known quantities, a task which could prove impossible, considering the experimental uncertainties on the measured observables. One way to increase the number of observables, at least for certain angles, was provided by the Pauli principle, which leads to symmetry/antisymmetry relations with respect to 90° c.m. for the amplitudes. This has two consequences : the amplitudes have to be determined only over one half of the total angular range, and observables at a given angle $(\pi - \theta)$ can be expressed by means of the amplitudes at angle θ. Consequently, provided that the polarimeter asymmetries have been measured

$\theta_{c.m.}$[deg.]	447 MeV	515 MeV	580 MeV
52.50	-0.0213 ± 0.0084	-0.0246 ± 0.0078	-0.0147 ± 0.0044
57.50	-0.0041 ± 0.0069	-0.0179 ± 0.0056	-0.0124 ± 0.0040
62.50	-0.0247 ± 0.0066	-0.0130 ± 0.0062	-0.0186 ± 0.0044
67.50	-0.0222 ± 0.0059	-0.0152 ± 0.0058	-0.0247 ± 0.0047
72.50	-0.0288 ± 0.0071	-0.0154 ± 0.0063	-0.0183 ± 0.0051
77.50	-0.0164 ± 0.0082	-0.0292 ± 0.0077	-0.0129 ± 0.0054
82.50	-0.0287 ± 0.0103	-0.0131 ± 0.0091	-0.0068 ± 0.0058
87.50	0.0099 ± 0.0153	-0.0140 ± 0.0137	-0.0049 ± 0.0071
92.50			-0.0077 ± 0.0091
93.75	-0.0185 ± 0.0092	0.0043 ± 0.0113	
97.50			-0.0049 ± 0.0073
101.25	-0.0189 ± 0.0067	-0.0079 ± 0.0084	
102.50			-0.0118 ± 0.0069
107.50			0.0039 ± 0.0064
108.75	-0.0032 ± 0.0053	-0.0071 ± 0.0074	
112.50			0.0020 ± 0.0058
116.25	-0.0030 ± 0.0049	-0.0012 ± 0.0058	
117.50			-0.0057 ± 0.0054
122.50			-0.0078 ± 0.0049
123.75	-0.0027 ± 0.0050	-0.0045 ± 0.0049	
127.50			-0.0033 ± 0.0045
131.25	-0.0172 ± 0.0043	0.0030 ± 0.0050	
132.50			-0.0023 ± 0.0043
137.50			-0.0035 ± 0.0040
138.75	-0.0107 ± 0.0063	0.0012 ± 0.0055	
142.50			0.0026 ± 0.0040
146.25	0.0298 ± 0.0333	-0.0234 ± 0.0151	
147.50			-0.0024 ± 0.0048

Table 4: Same as Table 1 but for $\varepsilon_{2s}(Z)$.

at θ and $(\pi - \theta)$, one can also use the 10 asymmetries at $(\pi - \theta)$ to fit the amplitudes and analysing powers at θ, while only 3 new free parameters – the 3 polarimeter analysing powers at $(\pi - \theta)$ – had to be introduced in the analysis. This condition was fulfilled for 8 angles between 0° and 90° c.m. leading to the reasonably safe situation of having a well overdetermined set of 27 equations at our disposal, for 17 unknowns.

4 The Effect of a Change of the Sign of the l and s Polarizations of the Proton Beam on the Amplitudes

4.1 The effect on the amplitude analysis

Our confidence in the first analysis was principally based on three reasons :

i) The solution found for the amplitudes was unique, stable and with a χ^2/d.o.f. of about 1.5.

ii) The amplitudes found were reasonably close to the calculations of Locher and Švarc [7] which became available shortly before the achievement of the reconstruction.

iii) The effective polarimeter analysing powers which came out from the analysis were in good agreement with the only comparable data available, obtained at Saturne by Garçon and collaborators [8]. with an experimental apparatus rather similar to the Geneva polarimeter

But there existed no experimental data with which our results could be compared.

One can see what is the effect of reversing the signs of the polarization parameters p_x et p_z. It is equivalent to applying the rotation $\mathcal{R}(0, \Pi, 0)$ of angle Π around the y axis to the initial state $|\alpha\beta>$, where α and β are the helicities of the incident and target protons, respectively. This transformation does not affect the spin correlation parameters but reverses the sign of the asymmetries $\varepsilon_s(X)$, $\varepsilon_s(Z)$, $\varepsilon_{2s}(X)$ and $\varepsilon_{2s}(Z)$ since these measurements were performed with an unpolarized target.
The $|\alpha\beta>$ states are transformed under rotation as follows :

$$\begin{aligned} \mathcal{R}(0,\Pi,0)|\alpha\beta> &= \sum_{\alpha'\beta'} \mathrm{R}^{\frac{1}{2}}_{\alpha'\alpha}(0,\Pi,0)\mathrm{R}^{\frac{1}{2}}_{\beta'\beta}(0,\Pi,0)|\alpha'\beta'> \\ &= \sum_{\alpha'\beta'} \mathrm{r}^{\frac{1}{2}}_{\alpha'\alpha}(\Pi)\mathrm{r}^{\frac{1}{2}}_{\beta'\beta}(\Pi)|\alpha'\beta'> . \end{aligned} \tag{1}$$

The amplitude

$$F^{\alpha\beta}_{\gamma} =< \gamma|F|\alpha\beta >, \tag{2}$$

with γ the deuteron helicity, will, then, be transformed under rotation as :

$$\mathcal{R}(F^{\alpha\beta}_{\gamma}) = \sum_{\alpha'\beta'} \mathrm{r}^{\frac{1}{2}}_{\alpha'\alpha}(\Pi)\mathrm{r}^{\frac{1}{2}}_{\beta'\beta}(\Pi) < \gamma|F|\alpha'\beta' > . \tag{3}$$

Given the values of the following rotation matrices :

$$r^{\frac{1}{2}}_{\frac{1}{2}\frac{1}{2}}(\Pi) = r^{\frac{1}{2}}_{-\frac{1}{2}-\frac{1}{2}}(\Pi) = 0 \ ; \ r^{\frac{1}{2}}_{\frac{1}{2}-\frac{1}{2}}(\Pi) = -r^{\frac{1}{2}}_{-\frac{1}{2}\frac{1}{2}}(\Pi) = -1, \tag{4}$$

we have the following transformations :

$$\begin{aligned}
\mathcal{R}(F_\gamma^{\frac{1}{2}\frac{1}{2}}) &= <\gamma|F|_{-\frac{1}{2}-\frac{1}{2}}> = F_\gamma^{-\frac{1}{2}-\frac{1}{2}} \\
\mathcal{R}(F_\gamma^{-\frac{1}{2}-\frac{1}{2}}) &= <\gamma|F|_{\frac{1}{2}\frac{1}{2}}> = F_\gamma^{\frac{1}{2}\frac{1}{2}} \\
\mathcal{R}(F_\gamma^{\frac{1}{2}-\frac{1}{2}}) &= -<\gamma|F|_{-\frac{1}{2}\frac{1}{2}}> = -F_\gamma^{-\frac{1}{2}\frac{1}{2}} \\
\mathcal{R}(F_\gamma^{-\frac{1}{2}\frac{1}{2}}) &= -<\gamma|F|_{\frac{1}{2}-\frac{1}{2}}> = -F_\gamma^{\frac{1}{2}-\frac{1}{2}},
\end{aligned} \tag{5}$$

and finally, using also the relations due to parity conservation (equations (5.8) of ref. [1]), one obtains :

$$\begin{aligned}
\mathcal{R}(A) &= \mathcal{R}(F_1^{\frac{1}{2}\frac{1}{2}}) = F_1^{-\frac{1}{2}-\frac{1}{2}} = -C \\
\mathcal{R}(B) &= \mathcal{R}(F_0^{\frac{1}{2}\frac{1}{2}}) = F_0^{-\frac{1}{2}-\frac{1}{2}} = B \\
\mathcal{R}(C) &= \mathcal{R}(F_{-1}^{\frac{1}{2}\frac{1}{2}}) = F_{-1}^{-\frac{1}{2}-\frac{1}{2}} = -A \\
\mathcal{R}(D) &= \mathcal{R}(F_0^{-\frac{1}{2}\frac{1}{2}}) = -F_0^{\frac{1}{2}-\frac{1}{2}} = D \\
\mathcal{R}(E) &= \mathcal{R}(F_1^{-\frac{1}{2}\frac{1}{2}}) = -F_1^{\frac{1}{2}-\frac{1}{2}} = -F \\
\mathcal{R}(F) &= \mathcal{R}(F_1^{\frac{1}{2}-\frac{1}{2}}) = -F_1^{-\frac{1}{2}\frac{1}{2}} = -E.
\end{aligned} \tag{6}$$

The change of sign of the longitudinal and sideways polarizations of the proton beam, finally :

i) transforms amplitude A into -C and vice-versa

ii) transforms amplitude E into -F and vice-versa

iii) leaves amplitudes B and D unchanged.

This explains how one could obtain a mathematically good solution despite the wrong sign of some ε measurements. However, if we had had data close to 0°, we would probably have noticed the wrong behavior of E and F since E has to go to zero at 0°.

Moreover, the polarimeter analysing powers, being also present in the expression of asymmetries depending only on the normal polarization of the beam, were constrained by these asymmetries and, therefore, were unaffected by the reversal of sign.

4.2 The effect on the partial wave analysis

A partial wave analysis (PWA) had also been performed in ref. [1]. The formalism and equations used in the analysis are correctly given in eq. 5.19 to 5.29 of ref. [1]. In particular one notices that the angular dependence of the amplitudes is imposed by the d functions :

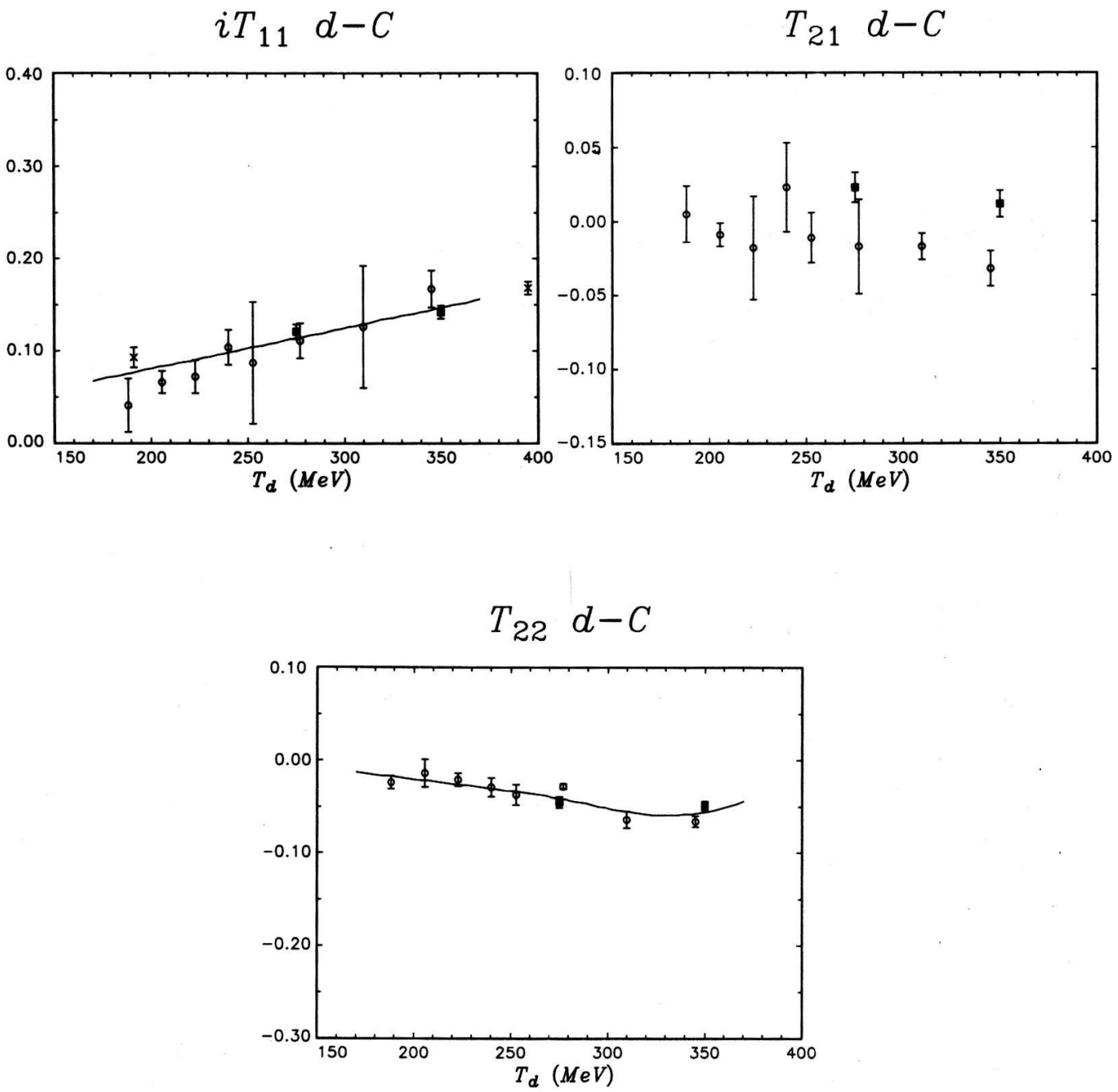

Figure 1: Polarimeter effective analysing powers iT_{11}, T_{21} and T_{22}. Open circles : this experiment; Crosses : ref. [8]; Full squares : ref. [10]. The curves are the results of the polynomial fits.

therefore the argument developed in Section 4.1 does not apply here. As a consequence all results concerning our PWA in ref. [1] have to be discarded, in particular table 18 and all the curves calculated with PWA solutions plotted in figs. 7 to 16. We did not repeat this analysis with the correct sign data as in the meantime such work was performed by D. Bugg [9].

5 The New Amplitude Analysis

After the sign correction was made, a new amplitude reconstruction was performed, in which two errors in equations (1.51) and (1.53) of ref. [1], concerning the transformation of the deuteron polarization from C.M to Lab systems, have been corrected. The correct relations are :

$$(1.51) \qquad L_{22}^{LAB} = (1/2)[(1+\cos^2\theta)L_{22}^{CM} + \sin(2\theta)L_{21}^{CM} + (\sqrt{3/2})\sin^2\theta L_{20}^{CM}] \quad (7)$$

$$(1.53) \qquad L_{21}^{LAB} = -(1/2)[\sin(2\theta)L_{22}^{CM} - 2\cos(2\theta)L_{21}^{CM} - (\sqrt{3/2})\sin(2\theta)L_{20}^{CM}] \quad (8)$$

Other errors, unfortunately, are present in ref. [1], but they turned out to be only misprints and had no effect on the analysis. Nevertheless, we take advantage of this article to give in an appendix the correct formulae.

The new analysis differs mainly from the previous one by the way the polarimeter effective analysing powers were treated. As it is said in section 3, apart from a measurement from Garçon and collaborators [8] at 191 and 395 MeV, there existed no experimental values for deuteron-Carbon analysing powers in our deuteron energy range when the first analysis was performed. Since then, the POMME polarimeter at Saturne II has been calibrated [10]. During the calibration run, POMME was set up in a configuration similar to the Geneva polarimeter, at two energies (275 and 350 MeV). One could take advantage of the precise data obtained for iT_{11} and T_{22}, shown in Table 5, to, somewhat, constrain the polarimeter analysing powers in our amplitude analysis.

	iT_{11}	T_{20}	T_{21}	T_{22}
275 MeV	.121±.008	-.016±.012	.023±.010	-.045±.006
350 MeV	.142±.007	-.014±.011	.012±.009	-.049±.005

Table 5: Effective d–C analysing powers of the Geneva polarimeter, measured with the POMME polarimeter at Saturne II, at 275 and 350 MeV.

In a first step, a solution for the amplitudes was sought, using the fitting program MINUIT [11], with the analysing powers left free. Out of 24 angles (8 angles × 3 energies), only 4 did not lead to convergence and were consequently rejected. A fit of the analysing powers values obtained in this procedure, to which were added the calibration data [10], and the values from ref. [8] for iT_{11}, was performed for iT_{11} and T_{22} under the form :

$$iT_{11}\,(T_{22}) = \sum_i a_i x^i \quad (9)$$

	iT_{11}	T_{22}		
		$T_d < 249.15$	$249.15 \leq T_d \leq 289.15$	$T_d > 289.15$
a_0	$-.22225$	$-.75637\ 10^{-1}$	$-.77280\ 10^{-1}$	$-.73184\ 10^{-1}$
a_1	$-.88146\ 10^{-3}$	$-.50046\ 10^{-3}$	$-.68099\ 10^{-3}$	$-.10347\ 10^{-2}$
a_2			$-.57328\ 10^{-5}$	$-.10798\ 10^{-5}$
a_3			$-.40650\ 10^{-7}$	$+.99005\ 10^{-7}$

Table 6: Coefficients of the polynomial fit of the deuteron polarimeter analysing powers.

	447 MeV	515 MeV	580 MeV
$d\sigma/d\Omega$	0.054	0.048	0.066
A_{yo}	1.275	0.614	1.981
A_{oy}	0.722	0.981	1.935
A_{xx}	0.749	0.679	0.916
A_{yy}	5.153	1.775	2.017
A_{zz}	0.365	1.040	0.628
A_{zx}	1.489	2.007	0.687
$\varepsilon_c(+y)\mid_\theta$	3.732	1.965	4.861
$\varepsilon_c(-y)\mid_\theta$	2.299	2.773	7.876
$\varepsilon_c(0)\mid_\theta$	2.186	2.979	5.335
$\varepsilon_{2c}(+y)\mid_\theta$	9.191	3.345	1.299
$\varepsilon_{2c}(-y)\mid_\theta$	4.844	1.021	2.575
$\varepsilon_{2c}(0)\mid_\theta$	5.295	1.946	1.013
$\varepsilon_s(X)\mid_\theta$	1.248	0.730	0.995
$\varepsilon_s(Z)\mid_\theta$	2.871	0.422	0.354
$\varepsilon_{2s}(X)\mid_\theta$	2.474	2.229	5.790
$\varepsilon_{2s}(Z)\mid_\theta$	14.451	1.157	1.088
$\varepsilon_c(+y)\mid_{(\pi-\theta)}$	2.699	0.451	2.849
$\varepsilon_c(-y)\mid_{(\pi-\theta)}$	2.195	1.459	2.363
$\varepsilon_c(0)\mid_{(\pi-\theta)}$	1.669	1.069	2.219
$\varepsilon_{2c}(+y)\mid_{(\pi-\theta)}$	4.765	8.344	6.576
$\varepsilon_{2c}(-y)\mid_{(\pi-\theta)}$	6.352	8.528	4.773
$\varepsilon_{2c}(0)\mid_{(\pi-\theta)}$	1.366	12.717	3.055
$\varepsilon_s(X)\mid_{(\pi-\theta)}$	2.293	2.218	0.196
$\varepsilon_s(Z)\mid_{(\pi-\theta)}$	1.571	4.789	0.795
$\varepsilon_{2s}(X)\mid_{(\pi-\theta)}$	6.729	10.717	3.563
$\varepsilon_{2s}(Z)\mid_{(\pi-\theta)}$	14.881	3.049	10.154
χ^2	102.918	79.052	75.959
χ^2/d.o.f.	1.286	0.988	0.949

Table 7: Contribution of individual observables to the χ^2.

$\theta_{c.m.}$	$\mid A \mid$	$\mid B \mid$	$\mid C \mid$	$\mid D \mid$	$\mid E \mid$	$\mid F \mid$
52.5	0.264±0.014	0.124±0.014	0.369±0.011	0.145±0.015	0.133±0.010	0.077±0.019
57.5	0.260±0.020	0.026±0.050	0.350±0.038	0.116±0.012	0.145±0.013	0.070±0.023
62.5	0.247±0.062	0.060±0.046	0.308±0.053	0.101±0.032	0.138±0.024	0.086±0.025
67.5	0.212±0.013	0.130±0.025	0.272±0.009	0.074±0.019	0.138±0.010	0.075±0.021
72.5	0.184±0.019	0.171±0.034	0.238±0.015	0.068±0.019	0.124±0.010	0.064±0.024
77.5	0.140±0.037	0.243±0.043	0.178±0.034	0.055±0.024	0.107±0.014	0.070±0.032
82.5	0.120±0.088	0.261±0.085	0.147±0.082	0.056±0.036	0.083±0.024	0.074±0.043
87.5	0.089±0.083	0.299±0.051	0.096±0.088	0.068±0.015	0.056±0.023	0.061±0.027

Table 8: Numerical values for the moduli of the $pp \rightarrow d\pi^+$ amplitudes at 447 MeV [$\sqrt{mb/sr}$].

$\theta_{c.m.}$	ϕ_B	ϕ_C	ϕ_D	ϕ_E	ϕ_F
52.5	6.178±0.426	3.007±0.639	2.149±0.617	2.508±0.634	1.377±0.854
57.5	0.643±0.122	3.169±0.187	2.114±0.169	2.630±0.161	1.095±0.313
62.5	2.148±0.362	2.955±0.517	1.849±0.475	2.378±0.511	0.856±0.436
67.5	2.752±0.395	2.977±0.535	1.501±0.508	2.367±0.534	0.877±0.473
72.5	3.031±0.363	2.924±0.485	1.324±0.472	2.313±0.492	1.014±0.409
77.5	3.076±0.305	3.071±0.414	0.786±0.399	2.440±0.453	1.195±0.373
82.5	3.127±0.319	3.093±0.465	0.660±0.459	2.442±0.632	1.371±0.474
87.5	3.356±0.436	3.555±0.560	0.851±0.488	2.310±0.636	1.635±0.613

Table 9: Numerical values for the phases of the $pp \rightarrow d\pi^+$ amplitudes at 447 MeV [*radians*].

$\theta_{c.m.}$	$\mid A \mid$	$\mid B \mid$	$\mid C \mid$	$\mid D \mid$	$\mid E \mid$	$\mid F \mid$
52.5	0.326±0.013	0.180±0.032	0.450±0.017	0.184±0.016	0.215±0.015	0.122±0.023
57.5	0.318±0.010	0.000±0.105	0.433±0.009	0.163±0.014	0.240±0.009	0.087±0.015
62.5	0.269±0.027	0.170±0.077	0.391±0.020	0.098±0.031	0.245±0.011	0.081±0.027
67.5	0.250±0.023	0.186±0.059	0.355±0.021	0.088±0.024	0.222±0.010	0.074±0.022
72.5	0.204±0.030	0.265±0.049	0.291±0.028	0.076±0.025	0.206±0.009	0.056±0.021
77.5	0.086±0.022	0.385±0.014	0.146±0.025	0.132±0.014	0.153±0.012	0.006±0.020
82.5	0.080±0.036	0.375±0.018	0.119±0.035	0.132±0.015	0.130±0.016	0.012±0.022
87.5	0.131±0.062	0.347±0.046	0.133±0.060	0.129±0.014	0.051±0.043	0.108±0.020

Table 10: Same as Table 8 but at 515 MeV.

$\theta_{\text{c.m.}}$	ϕ_B	ϕ_C	ϕ_D	ϕ_E	ϕ_F
52.5	0.066±0.181	2.827±0.263	2.072±0.252	2.262±0.263	0.425±0.298
57.5	4.390±0.061	2.964±0.078	1.772±0.087	2.330±0.079	0.245±0.139
62.5	3.127±0.404	2.970±0.534	1.217±0.602	2.314±0.549	6.123±0.613
67.5	3.117±0.336	2.940±0.445	1.245±0.535	2.348±0.454	6.011±0.599
72.5	3.010±0.235	2.943±0.306	0.482±0.412	2.396±0.323	5.936±0.628
77.5	2.596±0.228	2.346±0.245	5.744±0.249	1.601±0.268	4.984±3.476
82.5	3.083±0.235	2.845±0.268	6.186±0.260	2.261±0.319	2.052±2.024
87.5	6.129±0.326	3.182±0.459	3.058±0.353	3.759±0.570	5.038±0.449

Table 11: Same as Table 9 but at 515 MeV.

$\theta_{\text{c.m.}}$	$\lvert A \rvert$	$\lvert B \rvert$	$\lvert C \rvert$	$\lvert D \rvert$	$\lvert E \rvert$	$\lvert F \rvert$
52.5	0.270±0.013	0.154±0.034	0.539±0.016	0.136±0.029	0.326±0.012	0.195±0.015
57.5	0.241±0.014	0.142±0.040	0.507±0.016	0.155±0.017	0.298±0.010	0.183±0.012
62.5	0.224±0.017	0.155±0.034	0.466±0.015	0.169±0.025	0.268±0.014	0.162±0.014
67.5	0.193±0.017	0.264±0.028	0.379±0.017	0.122±0.025	0.270±0.011	0.145±0.014
72.5	0.163±0.024	0.306±0.030	0.312±0.021	0.153±0.023	0.220±0.013	0.141±0.016
77.5	0.125±0.049	0.336±0.040	0.252±0.028	0.190±0.028	0.172±0.019	0.109±0.035
82.5	0.074±0.032	0.375±0.020	0.175±0.026	0.208±0.017	0.145±0.016	0.058±0.024
87.5	0.054±0.020	0.397±0.018	0.074±0.041	0.226±0.019	0.098±0.023	0.058±0.028

Table 12: Same as Table 8 but at 580 MeV.

$\theta_{\text{c.m.}}$	ϕ_B	ϕ_C	ϕ_D	ϕ_E	ϕ_F
52.5	1.952±0.254	2.844±0.335	1.484±0.520	2.247±0.368	5.611±0.393
57.5	2.933±0.066	2.968±0.086	1.079±0.235	2.266±0.091	5.539±0.122
62.5	3.437±0.362	3.041±0.465	1.160±0.457	2.342±0.471	5.463±0.501
67.5	2.716±0.169	2.741±0.203	6.253±0.283	2.101±0.228	5.356±0.279
72.5	2.885±0.151	2.800±0.178	6.123±0.216	2.132±0.182	5.289±0.213
77.5	3.240±0.295	3.087±0.346	5.928±0.354	2.642±0.349	6.106±0.427
82.5	2.943±0.261	2.917±0.274	5.803±0.272	2.200±0.286	5.327±0.584
87.5	2.569±0.216	2.580±0.288	5.379±0.224	1.843±0.353	3.648±0.602

Table 13: Same as Table 9 but at 580 MeV.

where $x = T_d - 269.15$. T_d is the deuteron kinetic energy in MeV and 269.15 MeV is the middle of the deuteron kinetic energy range. A linear fit was sufficient for iT_{11}. For T_{22} one had to separate 2 regions. For $x < -20$ ($T_d < 249.15$ MeV) a linear fit was used while for $x > 20$ ($T_d > 289.15$ MeV) a 4–parameters fit was necessary. In the intermediate region, a 4–parameters polynomial was used to connect the two fits. Resulting coefficients are listed in table 6. Figure 1 displays the values obtained for iT_{11}, T_{21} and T_{22} in this first step, grouped in energy bins 20 MeV wide, together with the fits for iT_{11} and T_{22}.

In a second step, the amplitude reconstruction was performed with the analysing powers iT_{11} and T_{22} constrained around the values given by the fit, while T_{21} was forced to stay close to 0.

In both steps T_{20} was fixed to 0 for the following reasons :

i) It was experimentally shown that T_{20} was very small in all our deuteron energy range [8]. This was confirmed by the POMME calibration measurements.

ii) In the expressions relating the polarimeter asymmetries to the amplitudes and the polarimeter analysing powers, T_{20} appears at the denominator. Therefore, the analysis is very insensitive to this parameter. Indeed, by letting T_{20} freely vary, the χ^2 was not significantly improved, while T_{20} could take values unrealisticaly large.

The χ^2/d.o.f. of the solutions obtained was 1.29 at 447 MeV, 0.99 at 515 MeV and 0.95 at 580 MeV. Table 7 shows the contribution of individual observables to the total χ^2 at each energy.

The numerical results for the modules and phases of the amplitudes are given in Tables 8 to 13. The arbitrary overall phase has been chosen so that the phase of amplitude A is equal to 0.

6 Comparison with Theory

Figures 2 to 7 display the moduli and phases of the amplitudes compared to theoretical calculations due to Locher and Švarc [7,12] the Lyon group [13,14], Blankleider and Afnan [15], Niskanen [16], Rinat and Starkand [17] and one recent PWA due to Bugg, Hasan and Shypit [9] which includes our spin transfer data with the correct sign. To our knowledge, only two other PWA exist, from Watari, Hiroshige and Yonezawa [18] and Strakovsky, Kravtsov and Riskin [19], but they are older and do not include our spin transfer results. Also shown are the moduli of the amplitudes at 0° and 90° at 447 and 580 MeV from a previous work from the Geneva group [20].

Comparison between our results and the theoretical calculations call for the following remarks :

i) The difference between $|A|$ and $|C|$ increases with the energy and is systematically underestimated by the calculations.

ii) The largest discrepancies between the theoretical predictions are seen in amplitudes D, E and F and most of the calculations underestimate the moduli of these amplitudes.

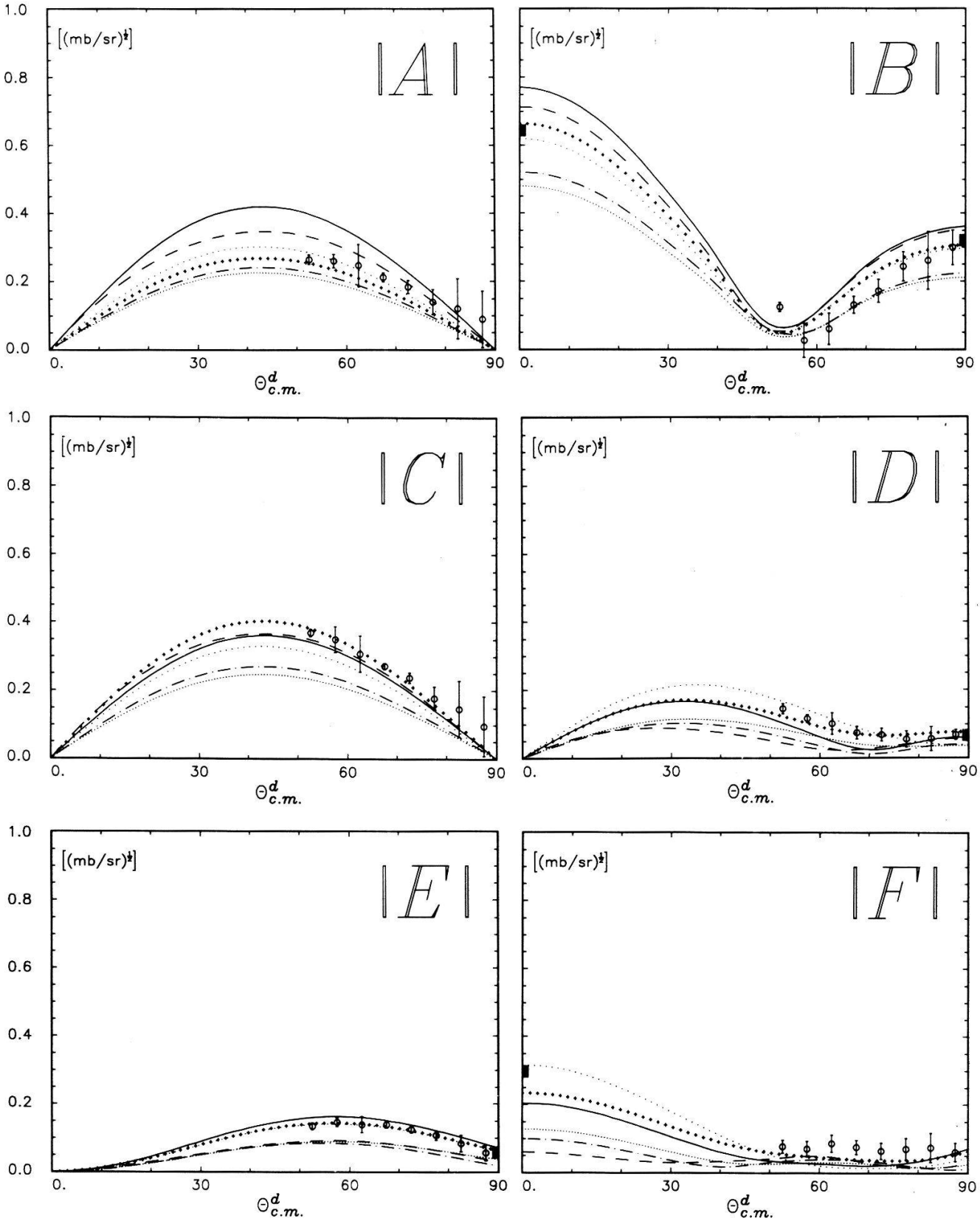

Figure 2: Plot of the moduli of the $pp \to d\pi^+$ amplitudes at 447 MeV. [7](– – – –), [13][14](————), [15](· – · – ·), [16](·····), [17](·····). Also shown is a PWA which includes our measurements [9](+++++++). The amplitudes at 0° and 90° are from [20].

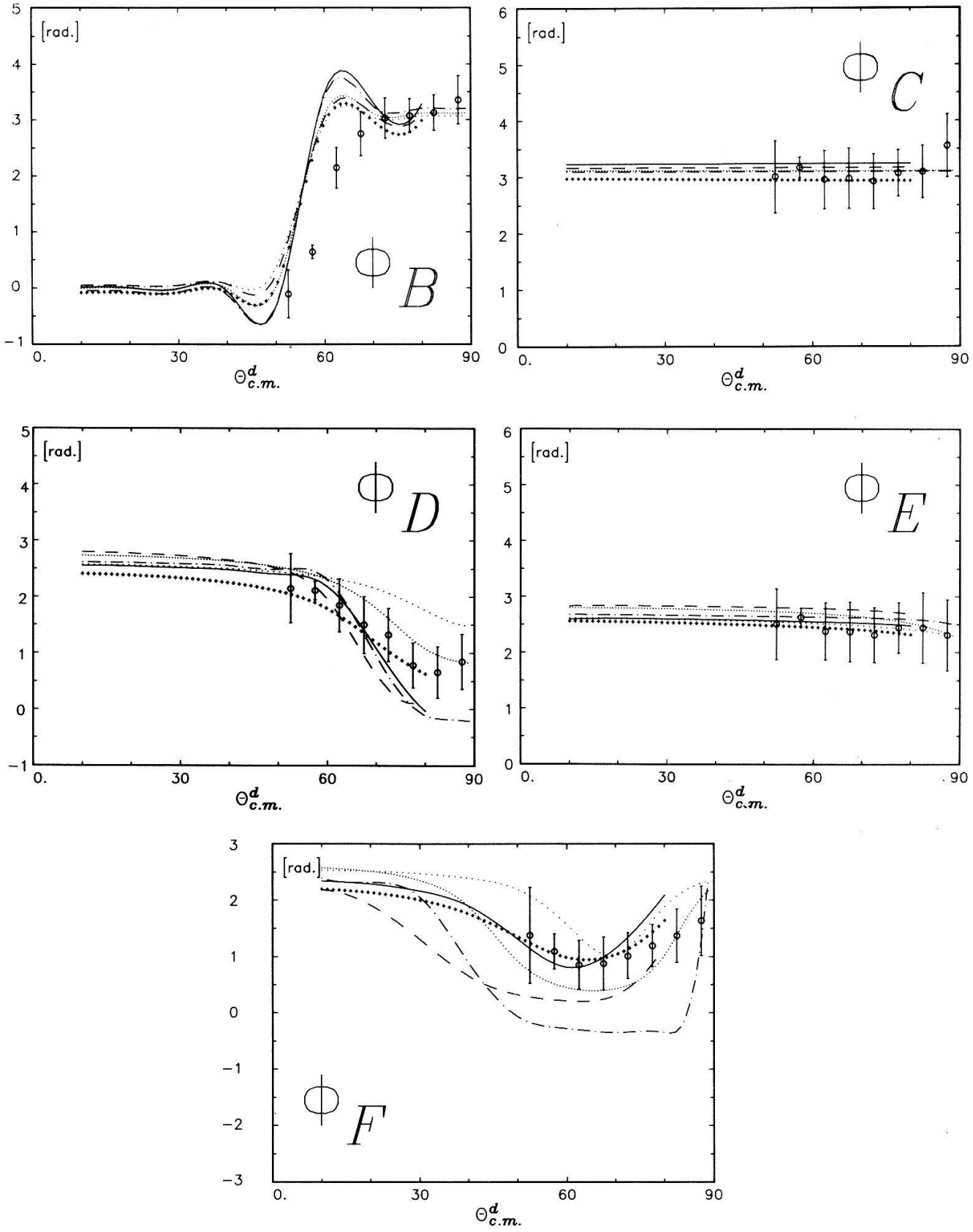

Figure 3: Plot of the phases of the $pp \to d\pi^+$ amplitudes at 447 MeV.

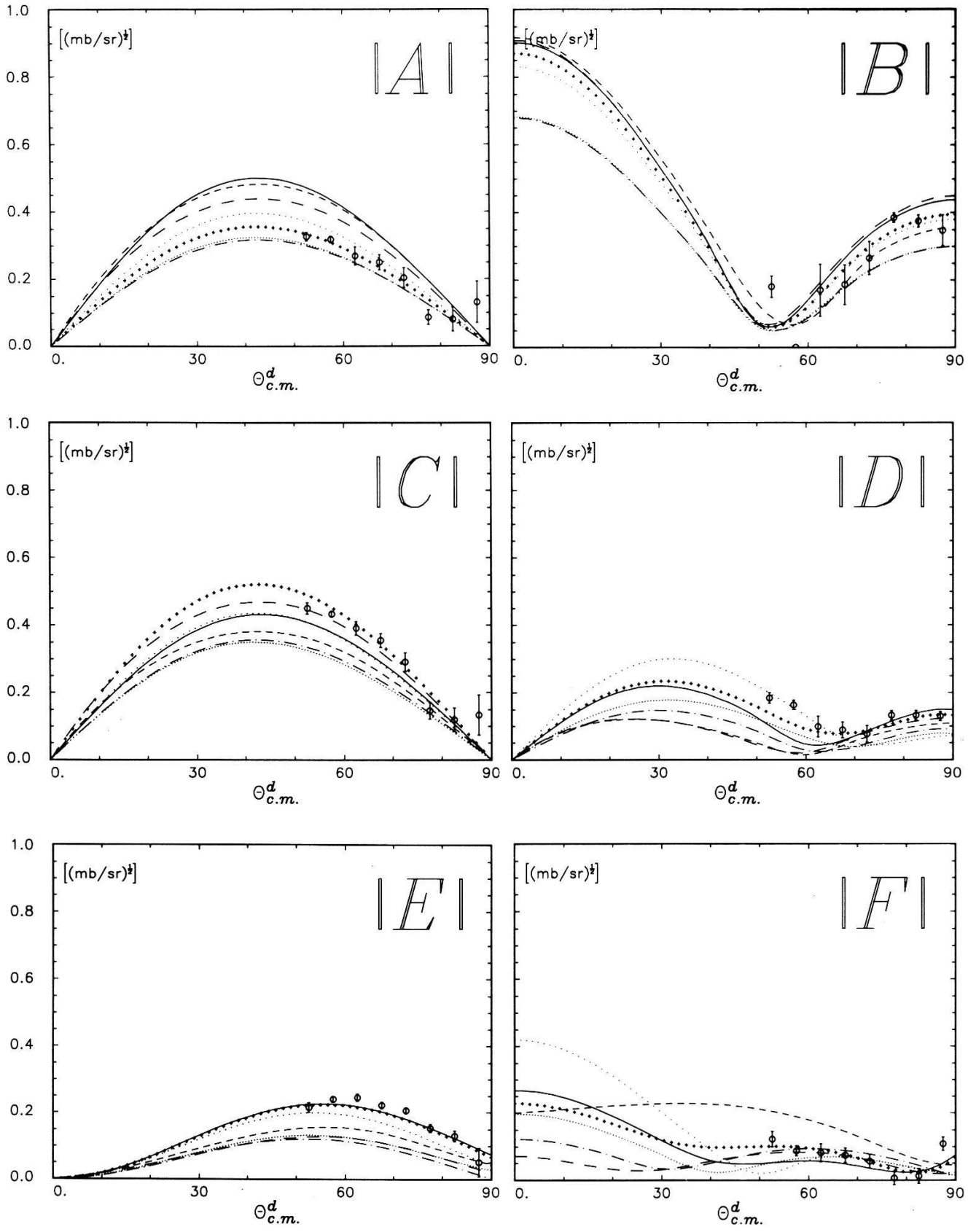

Figure 4: Same as Figure 2 but at 515 MeV, with predictions of ref. [12]((-------) as well.

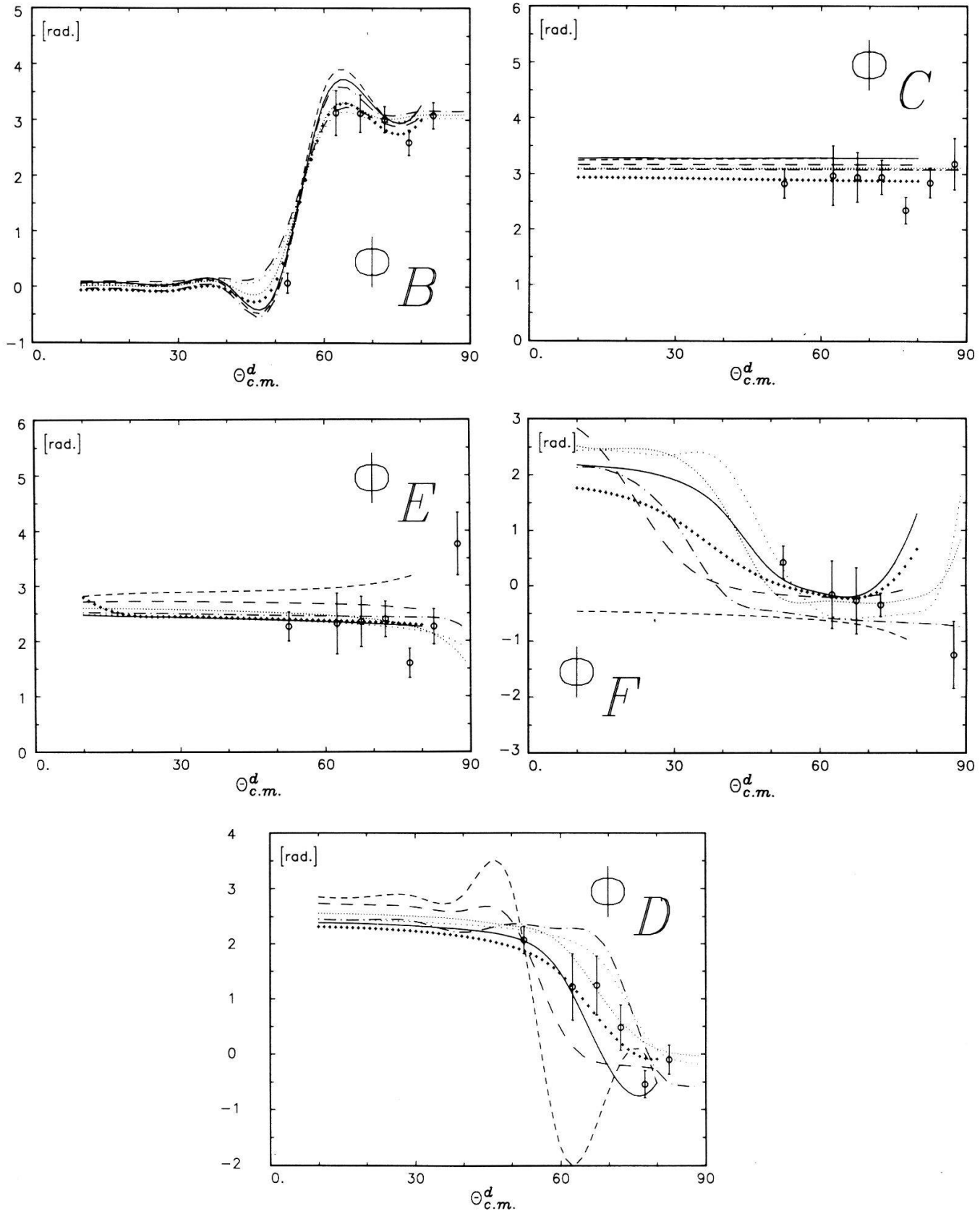

Figure 5: Same as Figure 3 but at 515 MeV, with predictions of ref. [12]((- - - - - - -) as well.

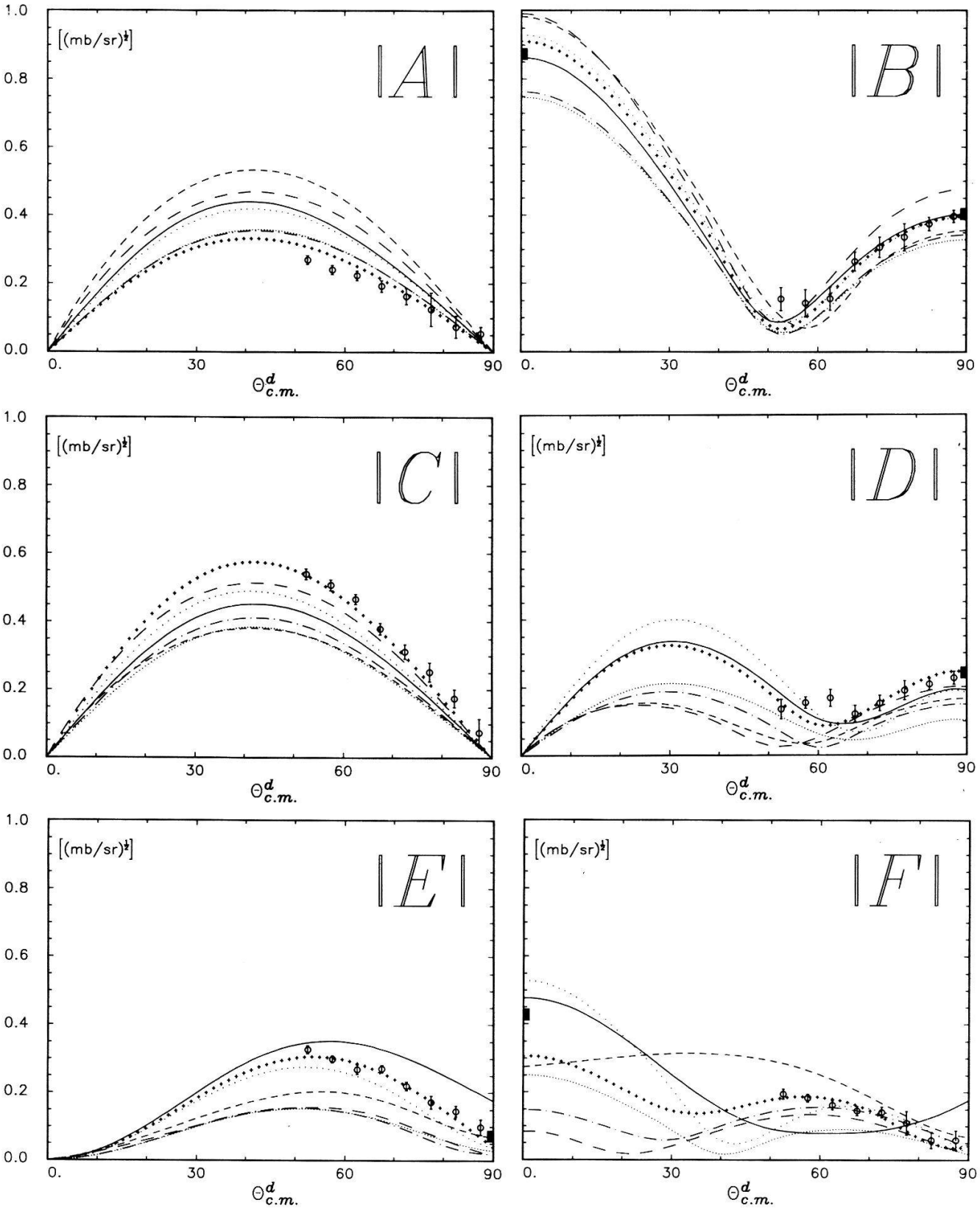

Figure 6: Same as Figure 4 but at 580 MeV.

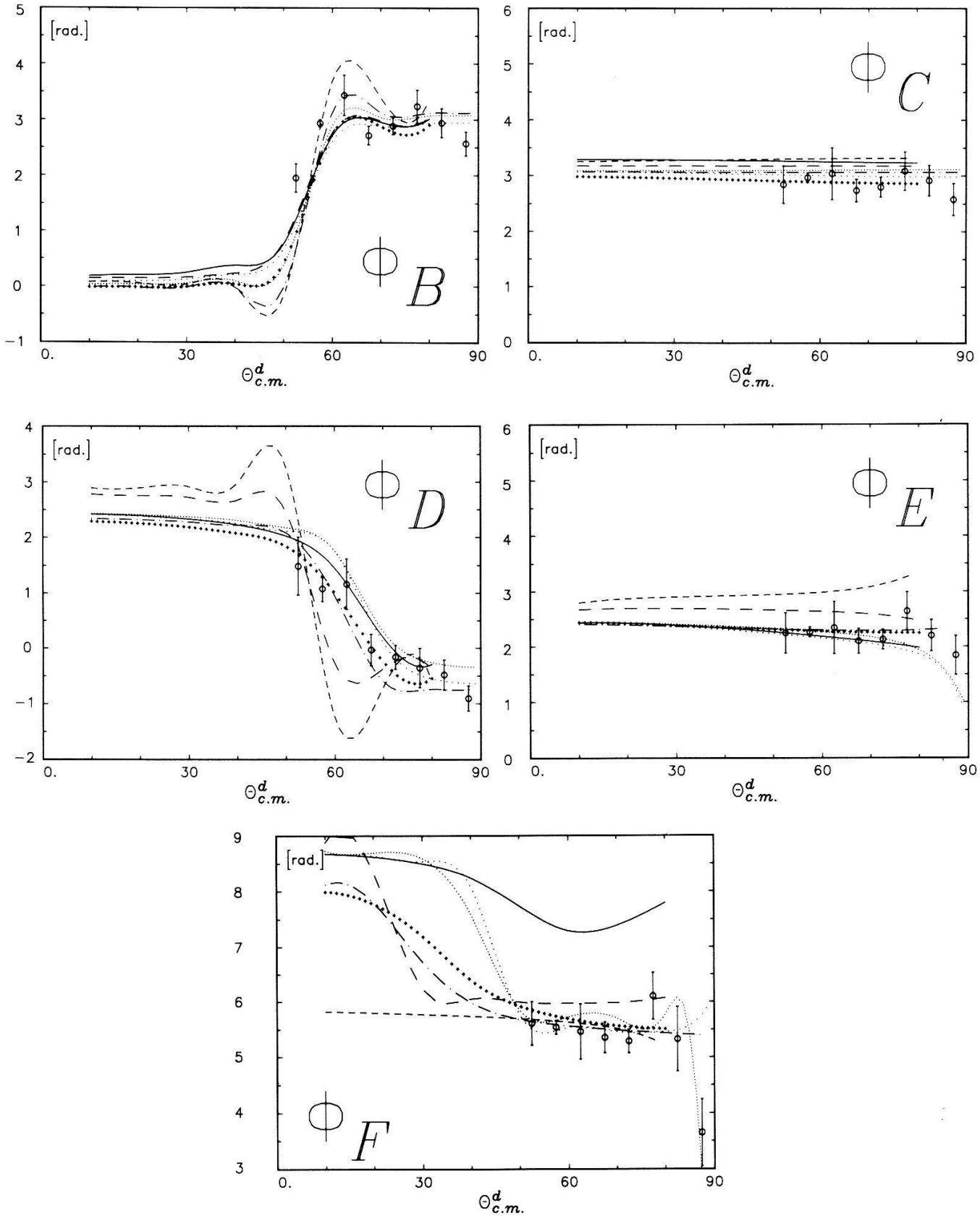

Figure 7: Same as Figure 5 but at 580 MeV.

These remarks confirm unambiguously the fact that the pp spin-triplet strength is too small in the different models, as already pointed out by Locher and Švarc [12]. Indeed, if one looks into the amplitudes definition, one can easily see that :

i) Amplitudes A, B and C are a mixing of pp singlet and triplet states, dominated by the singlet $^1D_2$, while D, E and F are pure triplet.

ii) In the limit of a null triplet strength, $\mid A \mid$ and $\mid C \mid$ are equal.

7 Conclusion

For the first time a direct, model–independent, reconstruction of the $pp \rightarrow d\pi^+$ scattering matrix has been performed at 447, 515 and 580 MeV. This task required the difficult measurement of the deuteron polarization by means of a carbon polarimeter in addition to the differential cross section, analysing powers and spin correlation coefficients measured at PSI by the Geneva group. The amplitudes obtained provide the most severe experimental constraint for theoretical calculations.

We are very much indebted to the TRIUMF group and especially to Dr. D. A. Hutcheon for many fruitful discussions which permitted us to uncover the sign reversal that had affected the analysis of our spin transfer data. Many different definitions for amplitudes and partial waves exist and we are very thankful to Prof. Garth Jones for having provided us with his code allowing their transformation into Blankleider's formalism [21]. Dr J. A. Niskanen has also been very helpful in this field and we want to thank him for this.

References

[1] G. Cantale et al. *Helv. Phys. Acta*, **60**(1987)398.

[2] E. Aprile et al. *Nucl. Phys.*, **A379**(1982)369.

[3] E. Aprile et al. *Nucl. Phys.*, **A415**(1984)365.

[4] D. A. Hutcheon et al. *Nucl. Phys.*, **A503**(1989)649.

[5] D. V. Bugg. Private communication.

[6] D. Aebischer et al. *Nucl. Phys.*, **B106**(1976)214.

[7] M. P. Locher and A. Švarc. *J. Phys. G*, **11**(1985)183.

[8] M. Garçon et al. *Nucl. Phys.*, **A458**(1986)287.

[9] D. V. Bugg, A. Hasan, and R. L. Shypit. *Nucl. Phys.*, **A477**(1988)546.

[10] B. Bonin et al. *N.I.M.*, **A288**(1990)389.

[11] F. James and M. Roos. MINUIT. CERN Library.

[12] M. P. Locher and A. Švarc. *Few Body Sys.*, **5**(1988)59.

[13] G. H. Lamot, J. L. Perrot, C. Fayard, and T. Mizutani. *Phys. Rev. C*, **35**(1987)239.

[14] C. Fayard et al. Few Body XII Vancouver 1989, G. H. Lamot private communication.

[15] B. Blankleider and I. R. Afnan. *Phys. Rev. C*, **31**(1985)1380.

[16] J. A. Niskanen. *Phys. Lett.*, **141B**(1984)301.

[17] A. S. Rinat and Y. Starkand. *Nucl. Phys.*, **A397**(1983)381.

[18] N. Hiroshige, W. Watari, and M. Yonezawa. *Prog. Theor. Phys.*, **72**(1984)1146.

[19] I. I. Strakovsky, A. V. Kravtsov, and M. G. Riskin. *Sov. J. Nucl. Phys.*, **40**(1984)273.

[20] E. Aprile-Giboni et al. *Nucl. Phys.*, **A415**(1984)391.

[21] B. Blankleider and I. R. Afnan. *Phys. Rev. C*, **24**(1981)1572.

Appendix

We take the opportunity of this new article to correct some errors which appeared in some of the equations of ref. [1].

(1.4) $$\rho_{\mu\mu'} = \rho^*_{\mu'\mu}$$

(1.6) $$\rho^I_{\mu\mu'} = \sum_{\nu\nu'} D^s_{\mu\nu}(\alpha,\beta,\gamma) D^s_{\mu'\nu'}(\alpha,\beta,\gamma)^* \rho^{II}_{\nu\nu'}$$

(1.9) $$t^I_{kq} = \sum_{q'} D^k_{qq'}(\alpha,\beta,\gamma)^* t^{II}_{kq'}$$

(1.10) $$t_{kq} = \mathrm{tr}(\rho\tau_{kq}) = \sum_{\mu\mu'} (\tau_{kq})_{\mu\mu'} \rho_{\mu'\mu}$$

(1.11) $$(\tau_{kq})_{\mu'\mu} = (2s+1)^{1/2}(-1)^{s-\mu} < s\mu', s-\mu \mid kq >$$

(1.16) $$\rho = \left(\sum_{kq} t_{kq} \tau^+_{kq} \right) / (2s+1)$$

(1.21) $$A^{k_a q_a k_b q_b}_{k_c q_c} = \mathrm{tr}\Big[F(\tau^{a+}_{k_a q_a} \otimes \tau^{b+}_{k_b q_b}) F^+ (\tau^c_{k_c q_c} \otimes \mathbf{1}_d) \Big] / \mathrm{tr}(FF^+)$$

(1.25) $$A^{k_a q_a k_b q_b}_{k_c q_c}(\theta; b(a,c)d) = (-1)^{q_a+q_b+q_c} A^{k_b q_b k_a q_a}_{k_c q_c}(\pi-\theta; a(b,c)d)$$

$I_0(\theta) = (\mathrm{d}\sigma/\mathrm{d}\Omega)\|_0(\theta)$	(s)
$A^{1B}(\theta) = A^{-1B}(\theta) = -A^{1T}(\pi-\theta) = -A^{-1T}(\pi-\theta)$	
$A^{11}(\theta) = A^{-1-1}(\theta),\ \ A^{1-1}(\theta) = A^{-11}(\theta),\ \ A^{00}(\theta)$	(s)
$A^{10}(\theta) = -A^{-10}(\theta) = -A^{01}(\pi-\theta) = A^{0-1}(\pi-\theta)$	
$t^0_{11}(\theta) = t^0_{1-1}(\theta),\ \ t^0_{21}(\theta) = -t^0_{2-1}(\theta)$	(a)
$t^0_{22}(\theta) = t^0_{2-2}(\theta),\ \ t^0_{20}(\theta)$	(s)
$A^{1B}_{11}(\theta) = A^{-1B}_{1-1}(\theta) = A^{1T}_{11}(\pi-\theta) = A^{-1T}_{1-1}(\pi-\theta)$	
$A^{1B}_{10}(\theta) = -A^{-1B}_{10}(\theta) = -A^{1T}_{10}(\pi-\theta) = A^{-1T}_{10}(\pi-\theta)$	
$A^{1B}_{1-1}(\theta) = A^{-1B}_{11}(\theta) = A^{1T}_{1-1}(\pi-\theta) = A^{-1T}_{11}(\pi-\theta)$	
$A^{0B}_{11}(\theta) = -A^{0B}_{1-1}(\theta) = -A^{0T}_{11}(\pi-\theta) = A^{0T}_{1-1}(\pi-\theta)$	
$A^{0B}_{10}(\theta) = A^{0T}_{10}(\pi-\theta)$	
$A^{1B}_{22}(\theta) = A^{-1B}_{2-2}(\theta) = -A^{1T}_{22}(\pi-\theta) = -A^{-1T}_{2-2}(\pi-\theta)$	
$A^{1B}_{21}(\theta) = -A^{-1B}_{2-1}(\theta) = A^{1T}_{21}(\pi-\theta) = -A^{-1T}_{2-1}(\pi-\theta)$	
$A^{1B}_{2-2}(\theta) = A^{-1B}_{22}(\theta) = -A^{1T}_{2-2}(\pi-\theta) = -A^{-1T}_{22}(\pi-\theta)$	
$A^{0B}_{22}(\theta) = -A^{0B}_{2-2}(\theta) = A^{0T}_{22}(\pi-\theta) = -A^{0T}_{2-2}(\pi-\theta)$	
$A^{0B}_{21}(\theta) = A^{0B}_{2-1}(\theta) = -A^{0T}_{21}(\pi-\theta) = -A^{0T}_{2-1}(\pi-\theta)$	
$A^{10}_{11}(\theta) = -A^{-10}_{1-1}(\theta) = A^{01}_{11}(\pi-\theta) = -A^{0-1}_{1-1}(\pi-\theta)$	
$A^{1-1}_{11}(\theta) = A^{-11}_{1-1}(\theta) = -A^{-11}_{11}(\pi-\theta) = -A^{1-1}_{1-1}(\pi-\theta)$	
$A^{11}_{11}(\theta) = A^{-1-1}_{1-1}(\theta),\ \ A^{00}_{11}(\theta) = A^{00}_{1-1}(\theta),\ \ A^{-11}_{10}(\theta) = -A^{1-1}_{10}(\theta),\ \ A^{-1-1}_{11}(\theta) = A^{11}_{1-1}(\theta)$	(a)
$A^{0-1}_{11}(\theta) = -A^{01}_{1-1}(\theta) = A^{-10}_{11}(\pi-\theta) = -A^{10}_{1-1}(\pi-\theta)$	
$A^{10}_{10}(\theta) = A^{-10}_{10}(\theta) = -A^{01}_{10}(\pi-\theta) = -A^{0-1}_{10}(\pi-\theta)$	
$A^{11}_{10}(\theta) = -A^{-1-1}_{10}(\theta)$	(s)
$A^{11}_{22}(\theta) = A^{-1-1}_{2-2}(\theta),\ \ A^{00}_{22}(\theta) = A^{00}_{2-2}(\theta),\ \ A^{-1-1}_{22}(\theta) = A^{11}_{2-2}(\theta),\ \ A^{1-1}_{20}(\theta) = A^{-11}_{20}(\theta)$	(s)
$A^{11}_{21}(\theta) = -A^{-1-1}_{2-1}(\theta),\ \ A^{-1-1}_{21}(\theta) = -A^{11}_{2-1}(\theta)$	(a)
$A^{11}_{20}(\theta) = A^{-1-1}_{20}(\theta),\ \ A^{00}_{20}$	(s)
$A^{10}_{22}(\theta) = -A^{-10}_{2-2}(\theta) = -A^{01}_{22}(\pi-\theta) = A^{0-1}_{2-2}(\pi-\theta)$	
$A^{1-1}_{22}(\theta) = A^{-11}_{2-2}(\theta) = A^{-11}_{22}(\pi-\theta) = A^{1-1}_{2-2}(\pi-\theta)$	
$A^{0-1}_{22}(\theta) = -A^{01}_{2-2}(\theta) = -A^{-10}_{22}(\pi-\theta) = A^{10}_{2-2}(\pi-\theta)$	
$A^{10}_{21}(\theta) = A^{-10}_{2-1}(\theta) = A^{01}_{21}(\pi-\theta) = A^{0-1}_{2-1}(\pi-\theta)$	
$A^{1-1}_{21}(\theta) = -A^{-11}_{2-1}(\theta) = -A^{-11}_{21}(\pi-\theta) = A^{1-1}_{2-1}(\pi-\theta)$	
$A^{0-1}_{21}(\theta) = A^{01}_{2-1}(\theta) = A^{-10}_{21}(\pi-\theta) = A^{10}_{2-1}(\pi-\theta)$	
$A^{10}_{20}(\theta) = -A^{-10}_{20}(\theta) = -A^{01}_{20}(\pi-\theta) = A^{0-1}_{20}(\pi-\theta)$	

Table 14: Explicit list of the 44 observables left after having applied parity conservation and the Pauli principle. (s) and (a) indicates when an observable is symmetric or antisymmetric. This table replaces table 2 of ref. [1]

(1.29) $$A_{kq}^{yB} = -(i/\sqrt{2})(A_{kq}^{1B} + A_{kq}^{-1B})$$

Table 2 has to be replaced by table 14 of this article.

(1.34) $$A_{kq}^{xy} = (i/2)(A_{kq}^{11} + A_{kq}^{1-1} - A_{kq}^{-11} - A_{kq}^{-1-1})$$

(1.36) $$A_{kq}^{yz} = -(i/\sqrt{2})(A_{kq}^{10} + A_{kq}^{-10})$$

in (1.50) $$\theta' = \theta_{LAB}\,|_{(\pi-\theta_{CM})}$$

(1.51) $$L_{22}^{LAB} = (1/2)[(1+\cos^2\theta)L_{22}^{CM} + \sin(2\theta)L_{21}^{CM} + (\sqrt{3/2})\sin^2\theta L_{20}^{CM}]$$

(1.53) $$L_{21}^{LAB} = -(1/2)[\sin(2\theta)L_{22}^{CM} - 2\cos(2\theta)L_{21}^{CM} - (\sqrt{3/2})\sin(2\theta)L_{20}^{CM}]$$

in (1.79) $$\pi^{11} = 2iC^{11}\ ;\ \pi^{20} = C^{20}\ ;\ \pi^{2q} = 2C^{2q}\ ,\ q = 1,2.$$

in (3.22), the coefficient of $\sin\Phi_C$ is : $-T^{11}L_{11} + T^{21}M_{21}$

(5.6) $$\mu_i = \frac{m_B.m_T}{m_B+m_T},\quad \mu_f = \frac{m_d.m_\pi}{m_d+m_\pi}$$

(5.12) $$4I_0A^{q'T} = \sum_{\alpha\gamma\beta\beta'} F_\gamma^{\alpha\beta}F_\gamma^{\alpha\beta'*}\left[(-1)^{1/2-\beta}\sqrt{2} < 1/2\beta', 1/2\ -\beta \mid 1q' >\right]$$

(5.14) $$4I_0A^{q'q''} = \sum_{\gamma\alpha\alpha'\beta\beta'} F_\gamma^{\alpha\beta}F_\gamma^{\alpha'\beta'*}\,[\,(-1)^{1-\alpha-\beta}\,2 < 1/2\alpha', 1/2\ -\alpha \mid 1q' > \times < 1/2\beta', 1/2\ -\beta \mid 1q'' >\,]$$

(5.15) $$4I_0t_{kq}^0 = \sum_{\alpha\beta\gamma\gamma'} F_\gamma^{\alpha\beta}F_{\gamma'}^{\alpha\beta*}\left[(-1)^{1-\gamma}\sqrt{3} < 1\gamma', 1\ -\gamma \mid kq >\right]$$

(5.18) $$4I_0A_{kq}^{q'q''} = \sum_{\alpha\alpha'\beta\beta'\gamma\gamma'} F_\gamma^{\alpha\beta}F_{\gamma'}^{\alpha'\beta'*}\,[\,(-1)^{1-\alpha-\beta}\,2 < 1/2\alpha', 1/2\ -\alpha \mid 1q' > \times < 1/2\beta', 1/2\ -\beta \mid 1q'' > \times(-1)^{1-\gamma}\sqrt{3} < 1\gamma', 1\ -\gamma \mid kq >\,]$$

in Table 11 : $$I_0A^{1T} = (i/\sqrt{2})\mathrm{Im}(AF^* + CE^* - BD^*)$$

$$I_0t_{20}^0 = (\sqrt{2}/4)(\mid A\mid^2 + \mid C\mid^2 + \mid E\mid^2 + \mid F\mid^2) - (\sqrt{2}/2)(\mid B\mid^2 + \mid D\mid^2)$$

in Table 15 : d_1, d_3, e_1, e_2, e_3 and e_4 have the wrong sign

in Figure 13 : A_{zx} is diplayed and not A_{xz}